Millennial variability of terrigenous transport to the central-southern Peruvian margin during the last deglaciation (18-13 kyr BP)

Marco Yseki, Bruno Turcq, Sandrine Caquineau, Renato Salvatteci, José Solis, C. Gregory Skilbeck, Federico Velazco, Dimitri Gutiérrez

Clim. Past, 18, 2255–2269, 2022
https://doi.org/10.5194/cp-18-2255-2022

Climate of the Past
Open Access
EGU

Millennial variability of terrigenous transport to the central–southern Peruvian margin during the last deglaciation (18–13 kyr BP)

Marco Yseki[1], Bruno Turcq[1], Sandrine Caquineau[1], Renato Salvatteci[2], José Solis[3], C. Gregory Skilbeck[4], Federico Velazco[5], and Dimitri Gutiérrez[3,5]

[1]IRD, LOCEAN-IPSL, Laboratoire d'Océanographie et du Climat: Expérimentation et Approches Numériques, Sorbonne Université, CNRS, IRD, MNHN, Paris, France
[2]Center for Ocean and Society, Kiel University, 24105 Kiel, Germany
[3]Laboratorio de Ciencias del Mar, Facultad de Ciencias y Filosofía, Universidad Peruana Cayetano Heredia, Lima, Peru
[4]Faculty of Science, University of Technology Sydney, P.O. Box 123 Broadway, Sydney, NSW, 2007, Australia
[5]Dirección General de Investigaciones Oceanográficas y de Cambio Climático, Instituto del Mar del Perú, Callao, Peru

Correspondence: Marco Yseki (marco.yseki@gmail.com)

Received: 14 December 2021 – Discussion started: 7 January 2022
Revised: 9 September 2022 – Accepted: 13 September 2022 – Published: 14 October 2022

Abstract. Reconstructing precipitation and wind from the geological record could help researchers understand the potential changes in precipitation and wind dynamics in response to climate change in Peru. The last deglaciation offers natural experimental conditions to test the response of precipitation and wind dynamics to high-latitude forcing. While considerable research has been done to reconstruct precipitation variability during the last deglaciation in the Atlantic sector of South America, the Pacific sector of South America has received little attention. This work aims to fill this gap by reconstructing types of terrigenous transport to the central–southern Peruvian margin (12 and 14° S) during the last deglaciation (18–13 kyr BP). For this purpose, we used grain-size distribution in sediments of marine core M77/2-005-3 (Callao, 12° S) and core G14 (Pisco, 14° S). We analyzed end-members (EMs) to identify grain-size components and reconstruct potential sources and transport processes of terrigenous material across time. We identified four end-members for both Callao and Pisco sediments. In Callao, we propose that the changes in the contributions of EM4 (101 µm) and EM2 (58 µm) mainly reflect the hydrodynamic energy and diffuse sources, respectively, while the variations in EM3 (77 µm) and EM1 (11 µm) reflect changes in the eolian and fluvial inputs, respectively. In Pisco, where there are strong winds and an extensive coastal desert, changes in the contribution of EM1 (10 µm) reflect changes in river inputs, while EM2 (52 µm), EM3 (75 µm), and EM4 (94 µm) reflect an eolian origin. At millennial scale, our record shows an increase in the fluvial inputs during the last part of Heinrich Stadial 1 (∼ 16–14.7 kyr BP) at both locations. This increase was linked to higher precipitation in the Andes related to a reduction of the Atlantic Meridional Overturning Circulation and meltwater discharge in the North Atlantic. In contrast, during the Bølling–Allerød interstadial (∼ 14.7–13 kyr BP), there was an eolian input increase, associated with stronger winds and lower precipitation that indicate an expansion of the South Pacific Subtropical High. These conditions would correspond to a northern displacement of the Intertropical Convergence Zone–South Pacific Subtropical High system associated with a stronger Walker circulation. Our results suggest that variations in river discharge and changes in surface wind intensity in the western margin of South America during the last deglaciation were sensitive to Atlantic Meridional Overturning Circulation variations and the Walker circulation on millennial timescales. In the context of global warming, large-scale increases in precipitation and fluvial discharge in the Andes as a result of a declining Atlantic Meridional Overturning Circulation and southward displacement of the Intertropical Convergence Zone should be considered.

1 Introduction

The last deglaciation, a period of global warming starting at the end of the Last Glacial Maximum (LGM, ∼ 19 kyr BP) to the early Holocene (11.7 kyr BP), is an outstanding period in the Earth's history that provides a better understanding of the mechanisms regulating regional climatic conditions as a consequence of global warming (Clark et al., 2012; Shakun et al., 2012). During the last deglaciation, variations in meltwater discharge in the North Atlantic and their consequent impact on the intensity of the Atlantic Meridional Overturning Circulation (AMOC) resulted in abrupt climatic changes on a millennial scale (McManus et al., 2004; Mulitza et al., 2017; Ng et al., 2018), which in turn caused changes in the meridional–oceanic temperature gradient as well as a meridional shift of the mean annual position of the Intertropical Convergence Zone (ITCZ; Cheng et al., 2012; Deplazes et al., 2013; McGee et al., 2014).

Numerous studies based on both continental and marine records have evaluated the effects of meltwater discharge and temperature variations in the North Atlantic on precipitation in tropical South America (TSA; e.g., Mollier-Vogel et al., 2013; Novello et al., 2017; Mulitza et al., 2017; Stríkis et al., 2015; Bahr et al., 2018). Most such studies have suggested wetter conditions in this region during cold events in the Northern Hemisphere, including Heinrich Stadial 1 (HS1, ∼ 18–14.7 kyr BP) and the Younger Dryas (YD, ∼ 12.9–11 kyr BP). This has been linked to a southern displacement of the ITCZ (e.g., Mollier-Vogel et al., 2013; Mulitza et al., 2017; Bahr et al., 2018) and an intensification of the South American monsoon in its southern domain (Novello et al., 2017; Stríkis et al., 2015) in response to the weakening of the AMOC and increased meltwater discharges into the North Atlantic. Conversely, during the Bølling–Allerød (B-A, 14.7–12.9 kyr BP), a warm period in the Northern Hemisphere, dry conditions developed in TSA (e.g., Mollier-Vogel et al., 2013; Novello et al., 2017; Mulitza et al., 2017) due to the strong AMOC, the more northerly position of the ITCZ, and the weakening of the South American monsoon.

However, most records covering the last deglaciation concern eastern South America (e.g., Cruz et al., 2005; Montade et al., 2015; Stríkis et al., 2015, 2018; Zhang et al., 2015; Novello et al., 2017, Mulitza et al., 2017; Bahr et al., 2018), while records from the western slope of the Andes (e.g., Baker et al., 2001a, b) and the Peruvian margin are scarce (e.g., Rein et al., 2005; Mollier-Vogel et al., 2013). Previous attempts to reconstruct changes in the precipitation in the western flank of the Andes using marine sediment records have given rise to contrasting results. In northern Peru (4° S), based on titanium (Ti) to calcium (Ca) ratios, Mollier-Vogel et al. (2013) suggest an increase in fluvial inputs during the HS1 and YD and reduced precipitation during the B-A. However, off Callao (12° S), no difference in fluvial inputs, based here on lithic content, between HS1 and BA is reported (Rein et al., 2005). The difference between the two records could be because of the changes in sediment transport at the two sites and/or the interpretation of the proxies used in these studies. In both studies, Ti/Ca ratio at 4° S (Mollier-Vogel et al., 2013) and lithic content at 12° S (Rein et al., 2005) were considered indicators of the fluvial inputs. The latter is generally true in northern Peru (4° S) where rainfall can reach 466 mm yr^{-1} (Lagos et al., 2008). However, other processes can be invoked in more arid regions: for example, in central–southern Peru where rainfall is scarce (less than 20 mm yr^{-1}; Lagos et al., 2008). Indeed, Briceño-Zuluaga et al. (2016) have shown that, during the last millennium, part of the detrital fraction of marine sediments collected off Pisco was also of eolian origin. According to Briceño-Zuluaga et al. (2016) eolian inputs off Pisco can contribute up to almost 50 % of the terrigenous fraction during some climatic periods (e.g., the Medieval Climatic Anomaly). These results are based on the grain-size distributions of terrigenous components in the sediment.

The grain-size distribution of Peruvian margin sediments is typically polymodal, and for this reason, it can provide information on sediment transport mechanisms and/or sediment sources (Briceño-Zuluaga et al., 2016). Eolian particle diameters are relatively coarser than fluvial ones, and if wind intensification occurs, eolian flow and the frequency of coarse particles (∼> 36 µm) would increase. Thus, the relative abundance of fluvial particles (∼ 6–14 µm) would reflect the precipitation and continental runoff (e.g., Stuut et al., 2002; Stuut and Lamy, 2004; Pichevin et al., 2005; Briceño-Zuluaga et al., 2016; Beuscher et al., 2017). Mathematical methods can be used to identify the grain-size components of polymodal sediments. For instance, end-member analysis (EMA) has been widely used to infer changes in fluvial and/or eolian inputs (e.g., Stuut et al., 2002, 2007, 2014; Stuut and Lamy, 2004; Weltje and Prins, 2003, 2007; Pichevin et al., 2005; Holz et al., 2007; Just et al., 2012; Beuscher et al., 2017; Humphries et al., 2017; Jiang et al., 2017).

The aim of the current work is to reconstruct at the millennial scale the transport (fluvial and eolian) and sedimentation of the terrigenous inputs off central–southern Peru (Callao and Pisco) during the last deglaciation. To achieve this, grain-size distributions from surface sediments and sediment cores (M77/2-005-3, Callao and G14, Pisco) were measured, and EMA was used to deconvolved them into subpopulations. Surface sediments were collected during normal conditions and during the 2017 coastal El Niño (April 2017). During the 2017 coastal El Niño, the flow of the Callao and Pisco rivers reached extremely high levels during austral summer 2017, especially during March 2017 (Guzman et al., 2020). Likewise, in the month of April 2017, wind surface anomalies were positive, especially in central and southern Peru (Echevin et al., 2018). Chamorro et al. (2018) found a quasi-linear relationship between surface wind and pressure gradient anomalies during the El Niño period in 1998. The alongshore pressure gradient anomalies in 1998 were caused by a

greater increase in near-surface air temperature off the northern coast than off the southern coast of Peru. This inhomogeneous sea surface warming is similar during El Niño 2017. Based on the above, the samples collected in April 2017 may reflect changes in fluvial and may represent eolian transport associated with coastal or eastern Pacific El Niño events.

In addition, as a proxy for fluvial vs. eolian inputs, we used the titanium / zirconium (Ti/Zr) record from X-ray fluorescence (XRF) analysis of the 106 KL core collected off Callao and described by Rein et al. (2005). In a subsequent step, Ti, Al, and Zr were measured in surface sediments at Callao and Pisco by inductively coupled plasma mass spectrometry (ICP-MS) to better interpret the XRF results. We postulate that changes in the AMOC intensity have modulated the variability of winds and precipitation in the western TSA, as inferred by changes in the grain-size distribution of marine sediment particles, at millennial timescales. Our work provides new information on sedimentation, types of transport, and sources of terrigenous inputs on the Peruvian margin during the last deglaciation, offering a better understanding of the mechanisms modulating these processes during past periods of global warming.

1.1 Regional setting

We focused on the central–southern part (12–14° S) of the Peruvian margin. Callao and Pisco are located onshore in the Lima Basin (Suess et al., 1987). This basin exhibits high productivity and anoxic conditions that are favored by an intense oxygen minimum zone between about 200 and 400 m depth (Cardich et al., 2019); hence, sediments are composed of fine grains, are rich in organic matter, and contain abundant diatoms. The general absence of bioturbation in some areas and during some time periods allows for the preservation of laminations and therefore their use as paleoceanographic records (e.g., Rein et al., 2005; Gutiérrez et al., 2006, 2009, 2011; Sifeddine et al., 2008; Salvatteci et al., 2014a, b, 2016, 2019; Briceño-Zuluaga et al., 2016). In Callao, muddy laminated areas are reported (Reinhardt et al., 2002), but sedimentary records collected in the OMZ core, off Pisco, show more continuous laminations than the records collected off Callao (e.g., Salvatteci et al., 2016, 2019).

The main transport of the detrital fraction of coarse silt and sand to the hemipelagic sediments in the Peruvian margin occurs by the action of winds (Scheidegger and Krissek, 1982). In contrast to Callao, Pisco is characterized by the presence of large coastal deserts, extreme aridity, and dust storms known as Paracas winds. During these sporadic sand storms, wind velocities can exceed 10–15 m s^{-1} (Briceño-Zuluaga et al., 2017); these storms are produced by the local intensification of alongshore surface wind and by alongshore pressure gradients (Briceño-Zuluaga et al., 2017). Moreover, in Pisco, an intense coastal upwelling linked to strong alongshore surface wind occurs (Dewitte et al., 2011; Gutiérrez et al., 2011; Rahn and Garreaud, 2013). The intensity of alongshore surface winds presents a seasonal variability, with stronger winds during austral winter and weaker winds during austral summer (Fig. 1). This seasonality is regionally linked to the displacements of the ITCZ–South Pacific Subtropical High (SPSH) system and locally to continental–oceanic and alongshore pressure gradients (Strub et al., 1998; Gutiérrez et al., 2011; Chamorro et al., 2018). In contrast to the coarser particles that are transported by winds, quartz-rich silt and clays are transported by rivers to the continental shelf (Scheidegger and Krissek, 1982). The central–southern Peruvian coast is characterized by very low annual precipitation (Callao, 14 mm yr^{-1} and Pisco, 2 mm yr^{-1}) and intermittent flows of coastal rivers (Lagos et al., 2008). However, during austral summer, there is an increase in river discharges associated with increased monsoon precipitation in the Andes (Garreaud et al., 2009; Vuille et al., 2012). Occasional floods occur and higher sediment discharges are associated with intense precipitation during extreme El Niño events (Bourrel et al., 2015; Morera et al., 2017; Rau et al., 2016; Guzman et al., 2020).

A large fraction of the particles smaller than 10 µm (desert aerosols) are transported beyond the continental shelf (Saukel et al., 2011). Therefore, the fine fraction of eolian origin in the continental shelf sediments is negligible, and the fine fraction of the continental shelf is largely dominated by fluvial inputs. On the other hand, coarser particles (e.g., > 40 µm) settle on the continental shelf (Scheidegger and Krissek, 1982). Once in the water column, the dispersion patterns of clays (< 4 µm) and fine silts (8–11 µm) coincides with the surface and subsurface currents, while the coarser fraction presents limited dispersion near the coast (Scheidegger and Krissek, 1982). Likewise, near-bottom processes and bottom topography exert considerable control over the dispersal of hemipelagic sediments on the Peruvian margin (Scheidegger and Krissek, 1982).

2 Materials and methods

2.1 Surface sediments, marine core, and age model

Surface sediments (0–0.5 cm) were collected in Callao ($N = 12$) and Pisco ($N = 9$) at depths of 92–178 and 120–311 m, respectively, by the Instituto del Mar del Peru during the years 2015 (December), 2016 (August and December), and 2017 (February, April, and August), specifically along transects perpendicular to the coast (Fig. S1 in the Supplement). Details of the sampling sites are given in Table S1 in the Supplement. The samples collected in April 2017 coincided with the occurrence of a coastal El Niño event and will be considered representative of "coastal El Niño" conditions hereafter. All the other samples will represent "normal" conditions.

Core M77/2-005-3 was retrieved from the southeastern Pacific continental slope (12°05 S, 77°40, 07 W; 214 m water depth, 1336 cm long) during the M77-2 expedition in 2008 (Fig. 1). Because we focus on the last deglaciation period,

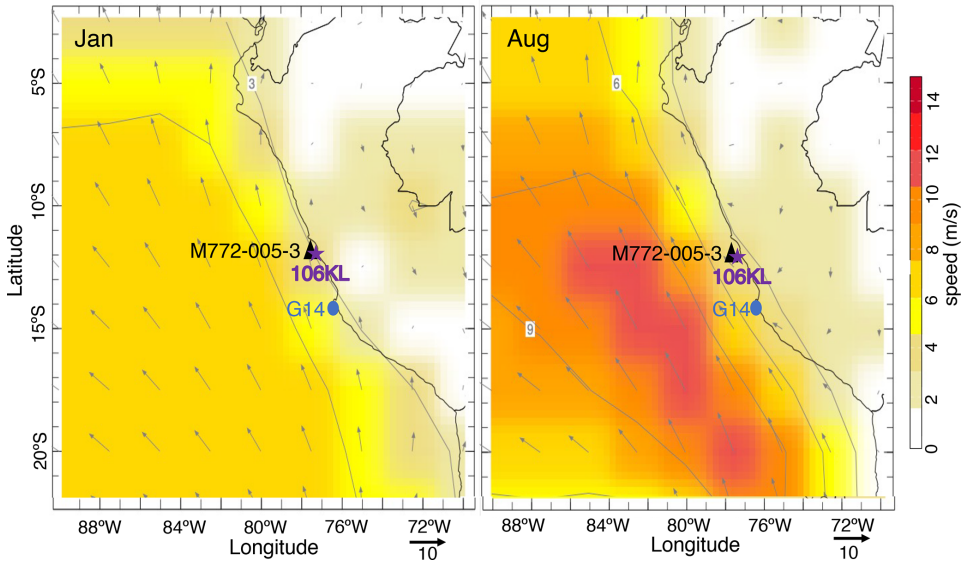

Figure 1. Location of the sampling of the sediment cores M77/2-005-3, 106 KL, and G14. Average wind speed ($m\,s^{-1}$) at 1000 hPa in January and August (http://iridl.ldeo.columbia.edu, last access: 17 March 2022).

we worked with the section from 0 to 700 cm core depth. A first depth–age model based on four ^{14}C ages was built by Salvatteci et al. (2019). In the present study, we added 22 ^{14}C ages and developed a new age depth–age model (Table S2). Radiocarbon measurements were performed on organic matter at the Laboratoire de Mesures du Carbone-14 (LMC14, Gif-sur Yvette, France). Ortlieb et al. (2011) reported a regional reservoir effect (ΔR) of 511 ± 278 years for the early Holocene (10.4–6.8 kyr), and in the absence of ΔR data for older periods, we used this value to calibrate the ^{14}C measurements for the last deglaciation as in Salvatteci et al. (2016, 2019). To construct the age model, we used the maximum probability ages obtained from the CALIB 8.1 software using the Marine 20 dataset. The chronological model based on the lineal model indicates that the examined section (0–700 cm) of core M77/2-005-3 (Fig. S2) recorded the LGM and the last deglaciation (22–13 kyr BP; 95–700 cm). Core M77/2-005-3 presents a hiatus at 94 cm, so a great part of the Holocene is missing.

Core G14 (14° S, 76° W; 390 m water depth) was retrieved during the Galathea-3 expedition in 2007 (Salvatteci et al., 2016). The radiocarbon dates of G14 were published in Salvatteci et al. (2016). For the current study, a new depth–age model based on a lineal model was developed with an updated calibration using the CALIB 8.1 software and the Marine 20 dataset. The upper part of sediment layers was not recovered in G14, which ranges from 13.4 to 24.6 kyr BP (Fig. S2).

The lithological descriptions of M77/2-005-3 and G14 are available in Salvatteci et al. (2016, 2019). The M77/2-005-3 and G14 cores show laminated and banded sediments with no evident signs of major discontinuities during the last deglaciation (Salvatteci et al., 2016, 2019). The G14 core presents more continuous laminated sediments compared with the M722-005-3 core (Salvatteci et al., 2016, 2019).

To compare our new data from cores M77/2-005-3 and G14 with previously published records in the area we modified the age model of core 106 KL (Rein et al., 2005). Core 106 KL (12°030 S, 77°39.80 W; 184 m water depth) was retrieved during cruise SONNE 147 (Rein et al., 2004, 2005). The chronology model and lithology have been fully described in Rein et al. (2004, 2005). A new depth–age model based on a lineal model was developed with an updated calibration using the CALIB 8.1 software and the Marine 20 dataset (Fig. S2), and we only used the sections covering the last deglaciation.

2.2 Grain-size distribution and end-member analysis

To reduce the effect of sediment disturbances that can produce artificial results, only laminated and banded sequences were subsampled for grain-size distribution analysis. Reworked sediments are widespread in the marine sediment records off Peru and can be distinguished from well-preserved sediments using X-ray images (Salvatteci et al., 2014b). For both surface and core sediment samples, to isolate the terrigenous fraction, we followed the procedure described in Briceño-Zuluaga et al. (2016). Organic matter, calcium carbonates, and biogenic silica were successively removed with hydrogen peroxide (H_2O_2 30 % at 60 °C for 3 to 4 d), hydrochloric acid (HCl 10 % for 12 h), and sodium carbonate (Na_2CO_3, 1 M at 90 °C for 3 h), respectively. The grain-size distribution was then measured using an auto-

mated image analysis system (model FPIA3000, Malvern Instruments), here with a measurement range of 0.5–200 µm. Further details on the FPIA3000 are described in Flores-Aqueveque et al. (2014) and Briceño-Zuluaga et al. (2016). Given that only particles smaller than 200 µm could be measured under the analytical conditions applied in the present work, all samples were sieved with a 200 µm mesh before being analyzed. Particles larger than 200 µm were not recovered in any sample; thus, our analysis covers the full range of grain sizes present in the surface and core sediments.

The grain-size distribution was generally plurimodal, and for this reason we used the AnalySize modeling algorithm (Paterson and Heslop, 2015) to deconvolute the grain-size distributions; the algorithm establishes a physical mixing model that transforms the measured particle size distribution histograms into the sum of a limited number of end-members (EMs) with a unimodal particle size distribution. The sum of determination coefficients (r^2), which represent the proportion of the variance of each EM against the total granulometric distribution, is calculated to estimate the minimum number of EMs necessary to reach a high percentage of the total variance. More specific details are available in Paterson and Heslop (2015).

2.3 ICP-MS analysis

The Al, Ti, and Zr concentrations in the surface sediments were determined by inductively coupled plasma mass spectrometry (ICP-MS; Agilent 7500 cx) after hot-plate acid digestion in polytetrafluoroethylene (PTFE) vessels. The employed acids (HF, HNO_3, and $HClO_4$) eliminated organic material and solubilized silicates (Jarvis et al., 1992). The complete protocol is described in detail in Salvatteci et al. (2014a). The accuracy of the concentration measurements was determined by comparison with MESS-3 (Marine sediment reference material, National Research Council of Canada). The relative standard deviation (RSD) estimated from duplicate analysis was less than 3.5 % for Al, Ti, and Zr.

2.4 XRF analysis

The piston core KL 106 was analyzed using an Avaatech XRF core scanner at the Marum Center (Bremen). Here, XRF scanning was done for 19 elements at 2 mm intervals. Ti is an aluminum- and silicate-related element and is associated mainly with clay minerals transported from the continent to the ocean through river discharges (Jansen et al., 1998; Yarincik et al., 2000). Conversely, Zr is predominantly enriched in heavy mineral species, particularly zircon. The latter is broadly distributed in natural sediments and typically has a relatively coarse grain size (Pettijohn, 1941). Zr has been widely used as a proxy for mean depositional grain-size variations (e.g., Dypvik and Harris, 2001; Wu et al., 2020). Using the Ti/Zr ratio, we compared Ti, which is present in all sizes of sediment but especially in clays, to Zr, which would only be present in the silt and sand fractions in the form of zircon minerals. Assuming that fine particles, such as clays, are mainly transported by rivers, while coarse particles (coarse silts and sands) come mainly from an eolian origin, the Ti/Zr ratio can be used as a potential proxy for fluvial versus eolian inputs.

3 Results

3.1 Grain-size distribution of the surface sediments

The grain-size distribution of all surface samples collected at the stations in Callao and Pisco are shown in Fig. 2. In Callao and Pisco, during normal conditions, the abundance of fine particles (< 10 µm) was higher at the deepest and furthest offshore stations than at coastal stations, while coarse particles (60–120 µm) were more abundant close to the coast (Fig. 2). Coarser particles were deposited mainly on the inner continental shelf because of their weight. During the 2017 coastal El Niño, a strong increase in fine particle (< 10 µm) abundance was found only at station E2 (Fig. 2a) in Callao. On the other hand, the abundance of the coarse fraction (50–100 µm) in the sediments from the most distant stations (E12 and E11) increased in Pisco (Fig. 2d and e).

The mean grain-size distribution per climatic period analyzed is shown in Fig. 3a and b. During the late HS1 (16–14.7 kyr BP), the abundance of fine particles (< 10 µm) was higher than during the early HS1 (18–16 kyr BP) and B-A in Callao and Pisco (Fig. 3a and b). This increase was more pronounced in Callao (Fig. 3a). On the other hand, during the B-A (14.7–13 kyr BP), the sediments were characterized by a high abundance of coarser particles (Fig. 3a and b).

3.2 End-member analysis

Based on a multiple correlation coefficient, a model with four EMs was chosen in Callao and Pisco, which explained 98 % and 95 % of the variance of the grain-size distribution dataset, respectively (Fig. 4a and b). The measured and modeled grain-size distributions were highly correlated (R^2: 0.86–0.99) for each analyzed sample, attesting to the fact that the use of four EMs was appropriate for our interpretation. Although a model with two EMs explained 95 % of the variance of the data in Callao, the variability of each EM's contribution was different (Fig. 6), suggesting that each EM indicated different processes or sources. Each of the four EMs presented a unimodal distribution, with the medians at 11 µm (EM1), 58 µm (EM2), 77 µm (EM3), and 101 µm (EM4) in Callao (Fig. 4c). In Pisco, each EM was represented by a unimodal distribution centered at 10 µm (EM1), 52 µm (EM2), 75 µm (EM3), and 94 µm (EM4; Fig. 4d).

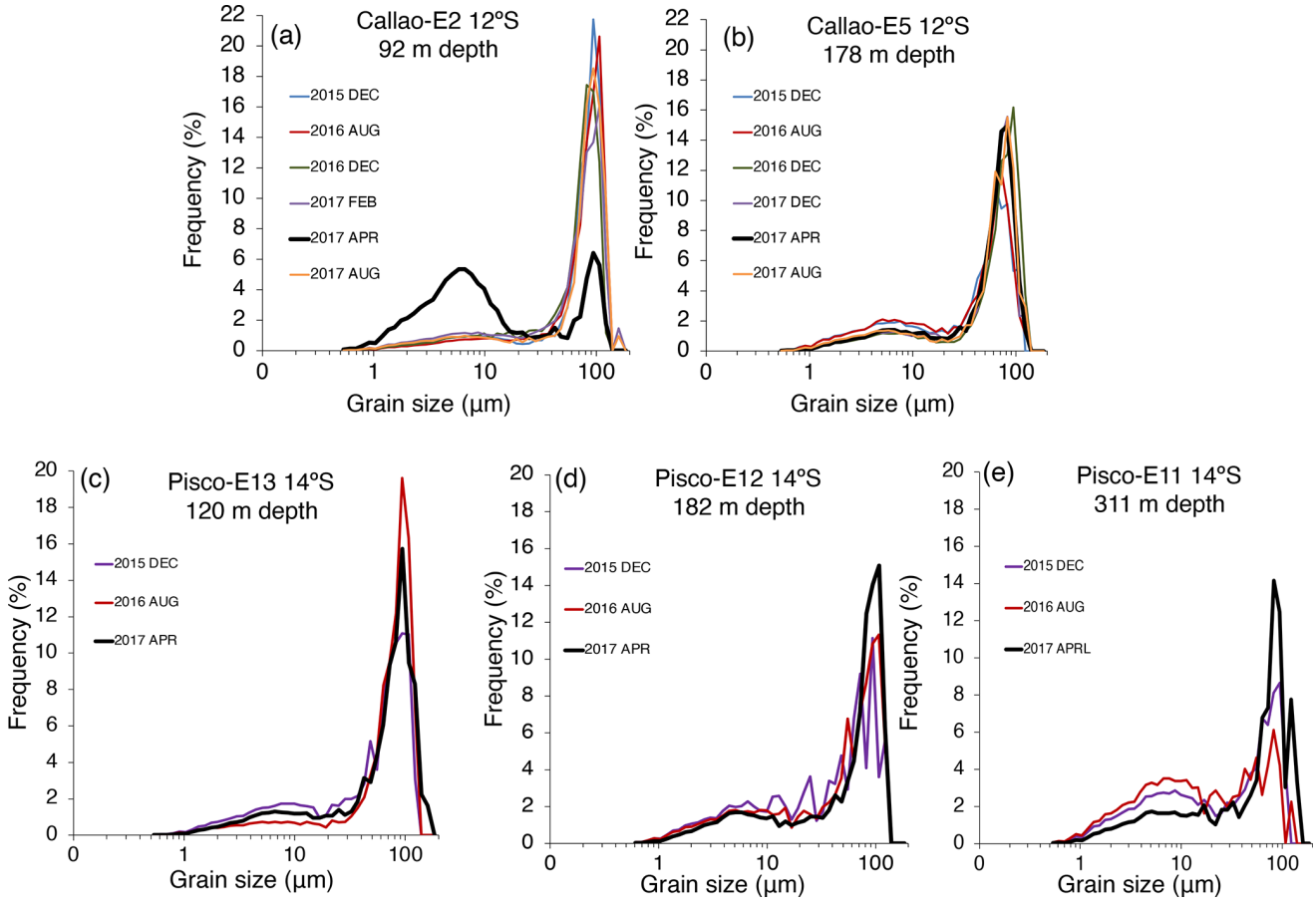

Figure 2. Grain-size distribution of surface sediments at the Callao **(a, b)** and Pisco stations **(c, d, e)**.

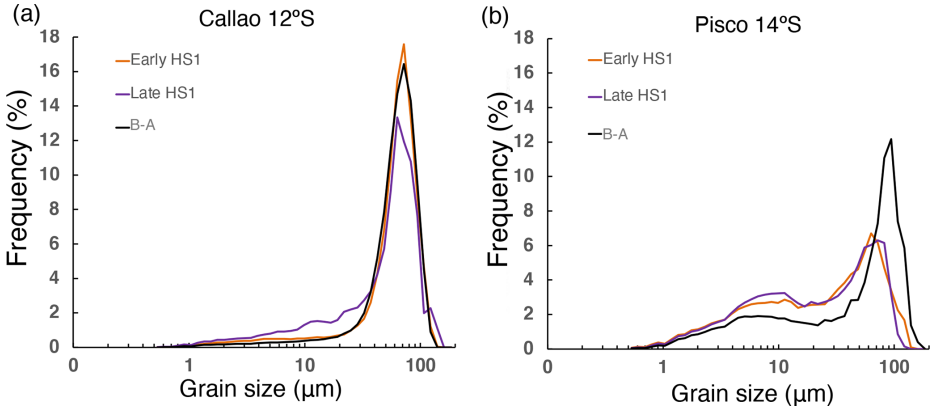

Figure 3. Mean grain-size distribution by climatic period in Callao **(a)** and Pisco **(b)**.

3.3 ICP-MS and XRF analysis

The concentrations of Al, Ti, and Zr, as well as the Ti/Zr ratio of the surface samples collected at Callao are presented in Fig. 5. The E2 station in Callao showed a very large increase in Ti and Al during the coastal El Niño (April 2017), with values twice the average of all other samples. This was related to the large number of fine particles measured that month in Callao. Regarding Zr, no significant difference between normal conditions and coastal El Niño was observed in E2 and E5 Callao. However, we found higher average Zr concentrations for E2 (46 ± 9 ppm) compared with E5 (34 ± 3 ppm) because the E2 station was closer to the coast and received more sandy inputs. Finally, the Ti/Zr ratio was

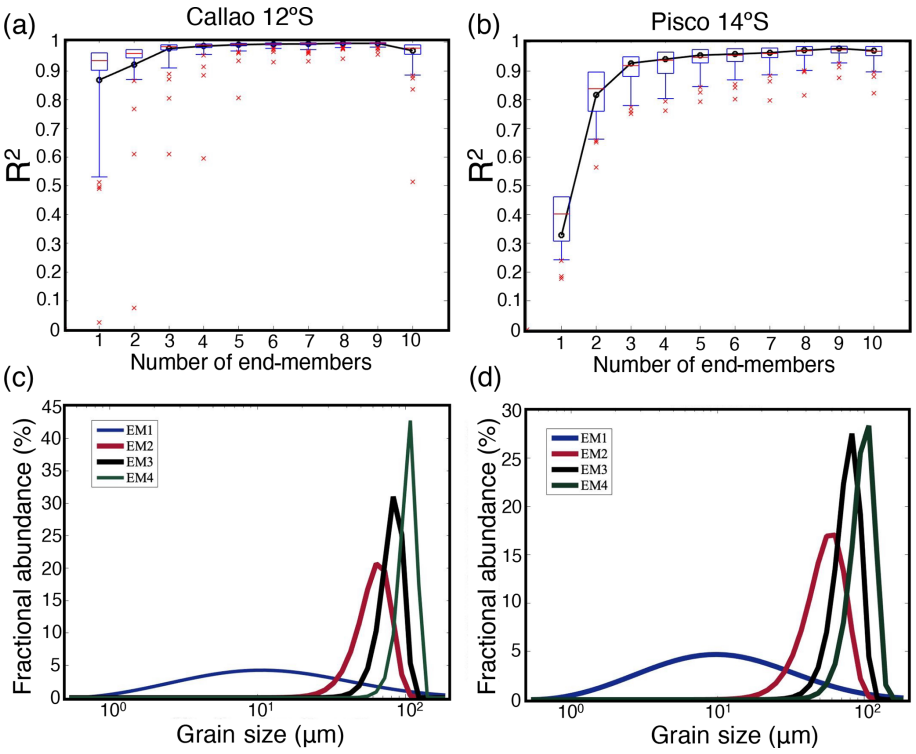

Figure 4. Coefficient of determination (r^2) as a function of the number of end-members chosen to model the observed grain-size distribution in Callao **(a)** and Pisco **(b)**. Grain-size distribution of the four end-members in Callao **(c)** and Pisco **(d)**.

1.7 times higher during the coastal El Niño (April 2017) with normal conditions at E2.

The Ti/Zr record of core 106 KL from Callao, which is used as a proxy for fluvial versus eolian inputs, shows millennial variability. During HS1, similar to the increment in fine particle abundance (Fig. 3a), Ti/Zr values were higher during late HS1 than during early HS1 (Fig. 7f). During B-A, a decreasing trend in the Ti/Zr ratio was demonstrated (Fig. 7f) by the increase in coarse particle abundance (Fig. 3a).

4 Discussion

4.1 Assignment of end-members

The terrigenous materials deposited on the Peruvian margin are transported by rivers and wind activity; however, there are also other diffused sources like the material produced by coastal erosion transported offshore by marine currents. The terrigenous sediments in Callao and Pisco are multimodal, which suggests that different processes are involved in the transport and deposition of these sediments. In both cores, we observed one end-member corresponding to a fine fraction (EM1) and three EMs corresponding to coarse fractions (EM2, EM3, and EM4). A previous study in Pisco used the variations of fine (10 µm) and coarse (50 and 100 µm) particles as proxies for river discharge and eolian inputs, respectively, for the last few centuries (Briceño-Zuluaga et al., 2016). However, the differences in the eolian sources, shelf and slope morphology, current intensity, and hydrodynamics between Callao and Pisco may modify the interpretation of the proxies described by Briceño-Zuluaga et al. (2016).

EM1 showed a mode at 11 and 10 µm in Callao and Pisco, respectively, which is consistent with the grain size of fine particles (∼ 6–14 µm) in marine sediments associated with river inputs reported in different areas of the world (e.g., Stuut and Lamy, 2004; Stuut et al., 2007; Beuscher et al., 2017) and Pisco (Briceño-Zuluaga et al., 2016). Indeed, the increase in fine particles (< 10 µm) and EM1 contribution in the surface marine sediments from E2 Callao (Figs. 2a and 6a) associated with local high fluvial discharges in Callao during the 2017 coastal El Niño (Guzman et al., 2020) corroborates the use of variations in the contribution of EM1 as an indicator of fluvial input changes. The non-increase in fine particles (as well as Al and Ti concentrations) in E5 Callao during the coastal El Niño was probably because of the greater distance between the fluvial source and the sampling site.

Previous studies in the southeastern Pacific used the abundance and fluxes of coarse particles (∼ 36–100 µm) in marine sediments as a proxy for wind intensity linked to the expansion and contraction of the SPSH (e.g., Flores-Aqueveque et al., 2015; Briceño-Zuluaga et al., 2016). Based on HYSPLIT (Hybrid Single-Particle Lagrangian Integrated Trajectory) simulations, Briceño-Zuluaga et al. (2017) have shown

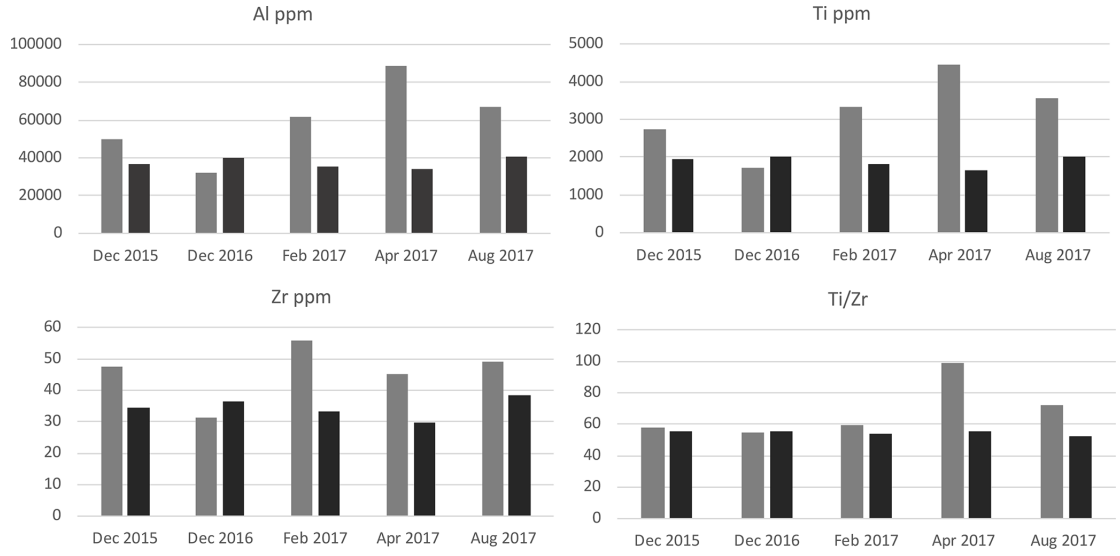

Figure 5. Al, Ti, and Zr concentration values in parts per million (ppm) and the Ti/Zr ratio of surface samples collected at Callao stations. Gray: E2 stations (92 m depth), black: E5 station (178 m depth).

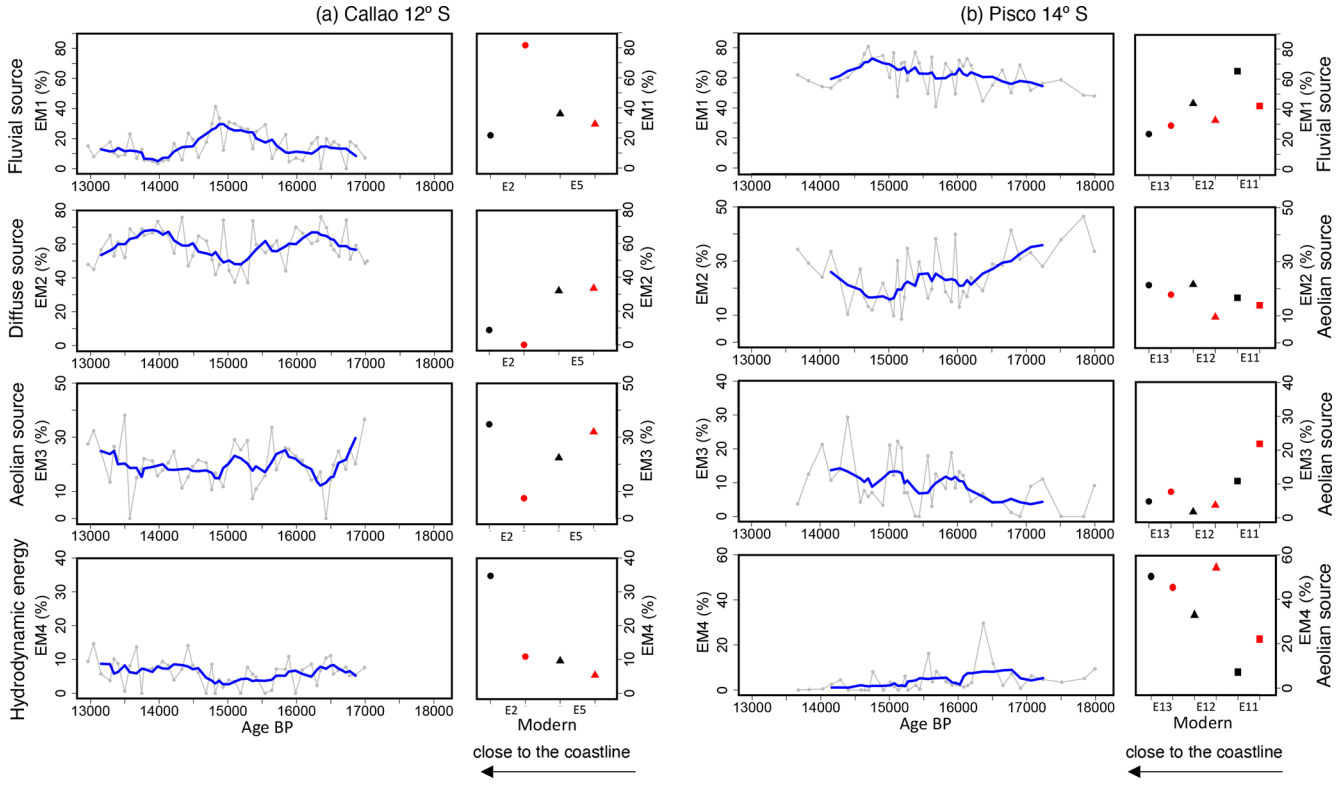

Figure 6. Variations in the contribution of the grain-size end-members from marine cores and surface sediments in Callao **(a)** and Pisco **(b)**. The modern period is represented by the mean end-member contribution of surface sediments collected during normal conditions (black symbols) and the coastal El Niño April 2017 event (red symbols).

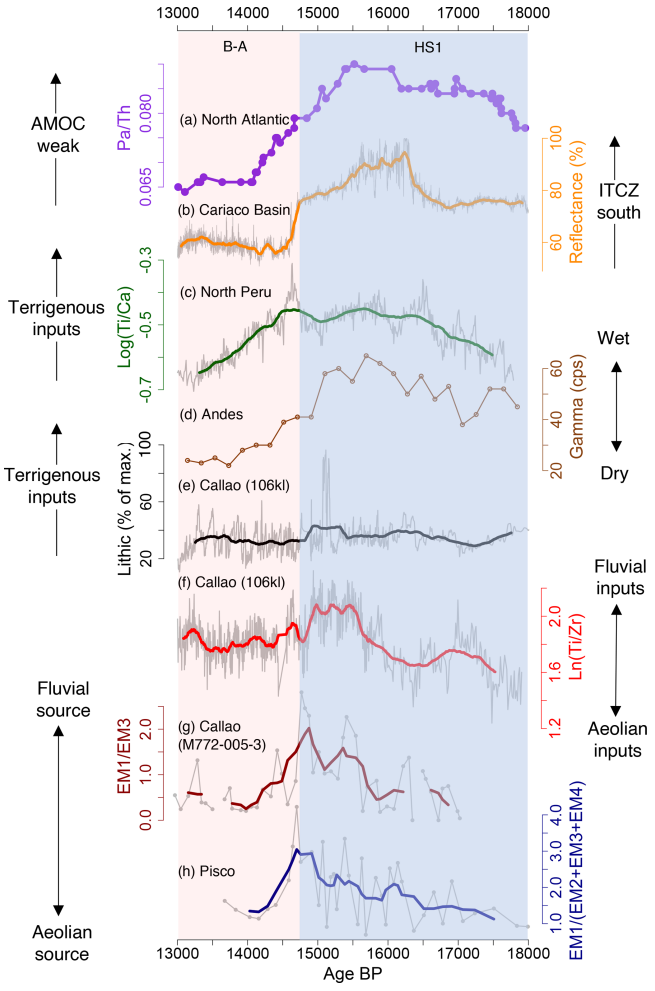

Figure 7. **(a)** Composite $^{231}Pa/^{230}Th$ record that reflects past changes in the AMOC (Ng et al., 2018). **(b)** Reflectance (%) from the Cariaco Basin as a proxy for the latitudinal displacement of the ITCZ (Deplazes et al., 2013). **(c)** Log (Ti/Ca) for core M77/2-059 from northern Peru (4° S; Mollier-Vogel et al., 2003). **(d)** Natural γ radiation as a proxy for effective moisture in the tropical Andes (Baker et al., 2021b). **(e)** Relative concentration of lithics for core 106 KL from Callao (Rein et al., 2005). **(f)** Ln (Ti/Zr) as a proxy for fluvial vs. eolian inputs in core 106 KL from Callao (this study). **(g)** EM1/EM2 ratio as a proxy for fluvial and eolian sources in Callao (this study). **(h)** EM1/(EM2 + EM3 + EM4) ratio as a proxy for fluvial and eolian sources in Pisco (this study).

that coarse particles (50–90 µm) can directly reach the continental shelf in Pisco during Paracas storms (characterized by wind velocities surpassing 10–15 m s^{-1}).

The EMs associated with the coarse fraction present similar modes in Callao and Pisco sediments (EM2 ∼ 55 µm, EM3 ∼ 75 µm, and EM4 ∼ 90–100 µm). Pisco is characterized by a large coastal desert and frequent dust storms. Also, because the shelf at Pisco is narrow, the distance from terrestrial sources that can be transported by winds did not vary significantly during the deglaciation compared with modern conditions. Based on this, particles between 50 and 90 µm (EM2, EM3, and EM4) can be interpreted as indicators of eolian input, as proposed by Briceño-Zuluaga et al. (2016). An increase in coarse particle abundance in Pisco surface sediments was recorded at the stations most distant from the coast, E12 and E11, during April 2017 (Fig. 2d and e), when wind stress along the coast was anomalously enhanced, especially in central and southern Peru (Echevin et al., 2018). This observation supports the hypothesis that these particles have an eolian origin and that the increase in their contribution suggests that, during events with stronger alongshore winds, these particles can be transported to a greater distance than during normal conditions, modifying their proportion in the sediments, but because of the small number of samples, this variation was not statistically significant (Fig. 2d and e). Finally, although EM2, EM3, and EM4 reflected an eolian source, their contribution variations during the last deglaciation were different (Fig. 6b). This can possibly be explained by changes in wind intensity; periods with stronger (weaker) winds result in an increase (decrease) in the amplitude of coarser particles.

In Callao, the context is different because there are no large deserts near the coast and dust storms are rare, so it is unlikely for ∼ 100 µm particles (EM4) to be transported directly to the sampling site. The presence of ∼ 100 µm particles could possibly be linked to bottom hydrodynamic processes. Indeed, during events of higher hydrodynamic energy, resuspension of fine particles and an increase in the relative frequency of coarser particles are expected. EM4 (101 µm) did not show drastic changes during the last deglaciation, suggesting that it did not influence the relative contribution of the other modes at the millennial scale (Fig. 6a). EM2 (58 µm) was found to be the dominant mode in Callao, ranging from 40 % to 80 % (Fig. 6a). Although these coarse sediments can be transported by winds (Briceño-Zuluaga et al., 2016, 2017), it is unlikely that this high percentage of coarse particles could be transported solely by the wind directly to the sampling site off Callao. It is more likely that ∼ 58 µm particles were derived from different sources (winds, coastal erosion) and are distributed on the continental shelf by the Peru–Chile Undercurrent (Reinhardt et al., 2002). In summary, based on the distance of the sampling site from the eolian sources, in addition to the absence of large eolian sources and dust storms in Callao, we propose that the changes in the contribution of EM2 and EM4 can be mainly related to other processes associated with diffuse sources and hydrodynamic energy, respectively. Conversely, EM3 can be seen as the best proxy for a wind source.

4.2 Millennial variability of fluvial and eolian inputs during the last deglaciation

The analysis of EMs allowed for a quantification of the main granulometric modes; however, because the sum of the contribution of the modes corresponds to 100 %, it is difficult

to consider the modes individually because an increase in one may reduce the others and influence their contribution variability. Thus, for a better visualization, a ratio between EMs indicative of a fluvial (EM1 in Callao and Pisco) and eolian (EM3 in Callao and the sum of EM2, EM3, and EM4 in Pisco) source will be used as a proxy for the variations in the fluvial and eolian inputs.

An increase in fluvial inputs based on the grain size and EMA was observed during the late HS1 ($\sim$ 16–14.7 kyr BP) with maximum values between $\sim$ 15.5 and 14.7 kyr BP in Callao (M77/2-005-3) and Pisco (G14; Fig. 7g and h).

Likewise, the Ti/Zr record in Callao (106 KL) indicated an increase in fluvial input during HS1, with maximum discharges between $\sim$ 15.5 and 14.9 kyr BP. The increment of Ti in surface sediments during higher fluvial discharges at Callao combined with the good relationship between the Ti/Zr record and the fluvial–eolian record (EM1/EM3) during the last deglaciation in Callao can support the idea that Ti, which is mostly linked to the fine fraction of marine sediments, is mainly transported by rivers to the Peruvian margin and can be used as a proxy for river discharge and precipitation (e.g., Mollier-Vogel et al., 2013; Salvatteci et al., 2014a; Fleury et al., 2015).

The contrasting differences between our record of fluvial input (based on grain size and Ti/Zr) and the record of lithic content based on reflectance (Rein et al., 2005) in Callao can be explained by the difference in the methodology and interpretation of the proxies. Rein et al. (2005) interpret the lithic content as a proxy for river discharges; however, as observed in our data (Fig. 6) and the literature (Briceño-Zuluaga et al., 2016), the terrigenous material can be transported to the central–southern Peruvian margin by different sources (e.g., fluvial and eolian), and the variability of fluvial and eolian transport follows different patterns, hence responding to different forcing.

Because heavy precipitation associated with the El Niño events in the Callao and Pisco coastal regions are occasional, a larger average fluvial discharge in Callao and Pisco would likely be related to precipitation fluctuations at higher elevations in the watersheds in the Andes. Previous studies suggest a correlation between North Atlantic cooling and massive meltwater discharges with increased precipitation in the central Andes (Baker et al., 2001a, b; Blard et al., 2011; Martin et al., 2018; González-Pinilla et al., 2021). During the last deglaciation, cooling in the North Atlantic and higher meltwater discharges generated a weakening of the AMOC (McManus et al., 2004; Mulitza et al., 2017; Ng et al., 2018). The latter generated an interhemispheric temperature contrast and an impact on precipitation in the central Andes associated with a southward shift of the ITCZ and an intensification of the South American monsoon in different regions: the central Andes (Baker et al., 2001a, b; Blard et al., 2011; González-Pinilla et al., 2021), southeastern (Cruz et al., 2005; Stríkis et al., 2015) and southwestern Brazil (Novello et al., 2017), and western Amazonia (Sublette Mosblech et al., 2012; Cheng et al., 2013). Indeed, the higher river discharges we evidenced in Callao and Pisco during late HS1 ($\sim$ 16–14.7 kyr BP) occurred simultaneously with the well-dated highstand of the giant paleolake Tauca ($\sim$ 16.6–14.5 kyr BP; Martin et al., 2018). Therefore, the increase and decrease in river discharges in central Peru during HS1 and B-A, respectively, could be explained by changes in precipitation in the Andes in response to changes in the intensity of the AMOC and meltwater pulses in the North Atlantic.

During the past few decades, the ITCZ in the eastern Pacific has shifted southward and generally narrowed and strengthened (Zhou et al., 2020). A recent study suggests a narrowing and southward shift of the ITCZ in the eastern Pacific in response to the SSP3-7.0 scenario by 2100 (Mamalakis et al., 2021). Although there are uncertainties about the effects of current global warming on AMOC intensity, there is evidence of the AMOC slowing over the past century (Rahmstorf et al., 2015; Caesar et al., 2018), and in climate model simulations of future climate change, the AMOC is projected to decline, generating a southward displacement of the ITCZ (Bellomo et al., 2021). In the context of global warming, large-scale precipitation and fluvial discharge increases in Peru related to AMOC decline and southward displacement of the ITCZ should be considered.

Concerning the variations in the eolian inputs and surface wind intensity in the Peruvian margin, changes in the intensity of the Walker circulation and meridional displacements of the ITCZ–SPSH system have been proposed as mechanisms to regulate surface alongshore winds and upwelling dynamics in the Humboldt Current System at multiple timescales (e.g., Gutiérrez et al., 2009; Briceño-Zuluaga et al., 2016; Salvatteci et al., 2014a, 2019). On centennial timescales, a northern displacement of the SPSH–ITCZ, here a response to a stronger Walker circulation, will cause an increase in alongshore winds and upwelling in the central–southern Peruvian margin (Salvatteci et al., 2014a; Briceño-Zuluaga et al., 2016). A sea surface temperature (SST) gradient increase in the equatorial Pacific indicates a more intense Walker circulation in B-A than during HS1 (Fig. 8a; Koutavas and Joanides, 2012). Moreover, a northern displacement of the ITCZ has also been recorded during B-A (Peterson et al., 2000; Deplazes et al., 2013). These conditions should have provoked an increase in the alongshore winds and eolian supply in central Peru during B-A. Indeed, in Callao and Pisco, the eolian inputs were the main transport from 14.7 to 13 kyr BP, suggesting, at least at the regional scale, an increase in alongshore wind and upwelling in central–southern Peru and an expansion of the SPSH (Fig. 8d and e). Our record of surface wind intensity variations and an alkenone-derived SST reconstruction based on alkenones (Salvatteci et al., 2019) in the same core collected from Callao showed similar trends (Fig. 8c). During HS1, a short cooling event between 16 and 15.5 kyr BP coincided with stronger alongshore winds (Fig. 8c and d). And, during the B-A, which was a cooling at 14.7–13 kyr BP, stronger eolian

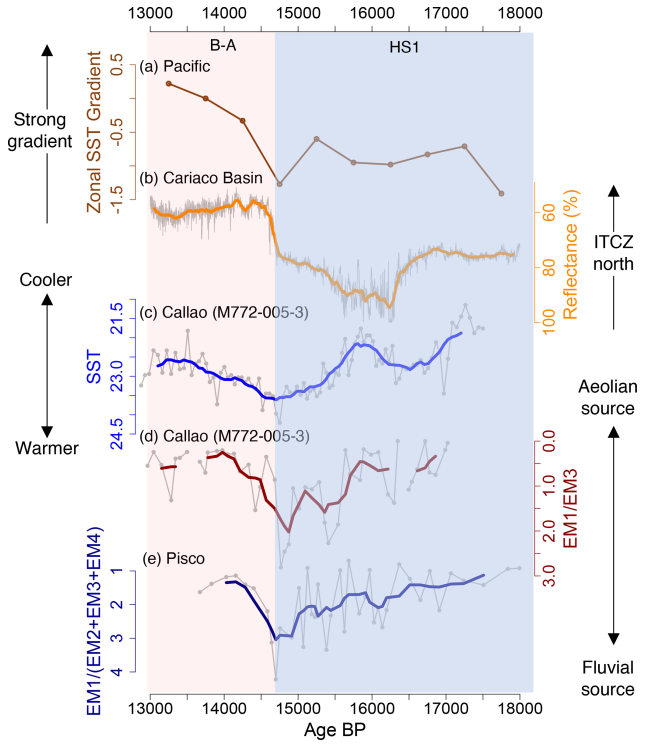

Figure 8. **(a)** Zonal SST gradient anomaly during the last deglaciation, calculated here as the difference between western and eastern Pacific averages (Koutavas and Joanides, 2012). **(b)** Reflectance (%) from the Cariaco Basin as a proxy for the latitudinal displacement of the ITCZ (Deplazes et al., 2013). **(c)** Alkenone-derived near-surface temperature from the M77/2-005-3 core in Callao (Salvatteci et al., 2019). **(d)** EM1 / EM2 ratio (reversal scale) as a proxy for fluvial and eolian sources in Callao (this study). **(e)** EM1/(EM2 + EM3 + EM4) ratio (reversal scale) as a proxy for fluvial and eolian sources in Pisco (this study).

transport associated with more intense alongshore winds occurred (Fig. 8c and d). These observations suggest that local processes as upwelling variations in response to changes in alongshore wind intensity may control SST variations during the last deglaciation, in addition to other processes such as the advection of the Southern Ocean and Antarctic climate signals by the Humboldt Current.

5 Conclusions

The variability of the grain-size distribution of marine sediments from the central–southern Peruvian margin (12 and 14° S) reveals millennial-scale changes in the transport and sedimentation processes of terrigenous material during the last deglaciation (18–13 kyr BP). We identified four granulometric EMs for both Callao and Pisco sediments, each of them reflecting different processes and sources and whose interpretation must take into consideration regional contexts. In the case of the Pisco core, located within the range of the eolian inputs, as has been shown earlier, the modes (EM2 to EM4) corresponded to eolian origin. In the case of the Callao core, which was located further from the coast and where sources of eolian particles are scarce, the EM2 and EM4 modes have been interpreted as reflecting local hydrodynamics, while EM3 represented the eolian supply. Our results support a tight relationship between high-latitude forcing and precipitation in the western flank of the Andes during the last deglaciation. During late HS1 (16–15 kyr BP), enhanced fluvial inputs in Callao and Pisco occurred and were associated with higher precipitation in the central Andes in response to the slowdown of AMOC and meltwater discharge in the North Atlantic. Finally, the increase in the eolian input during the B-A could be a result of stronger alongshore winds linked to a northern displacement of the ITCZ–SPSH system in response to a strong gradient of the Walker circulation. There is still uncertainty about the effects of current climate change; however, there is evidence of a slowing of the AMOC over the past century and in future climate model simulations. In the latter, the decline in the AMOC is accompanied by a southward shift in the ITCZ. Thus, we can probably expect an increase in precipitation and river flow in Peru in the future.

Data availability. The data associated with this paper will be submitted in the PANGAEA database upon publication of the paper.

Supplement. The supplement related to this article is available online at: https://doi.org/10.5194/cp-18-2255-2022-supplement.

Author contributions. MY, BT, and DG designed the study. MY and SC carried out the grain-size analysis. DG and CGS conducted the XRF analysis of core KL 106. FV collected the surficial samples, prepared them, and contributed to their interpretation. MY wrote the paper with the help of BT and SC. MY, BT, SC, RS, JS, CGS, FV, and DG discussed and commented on the paper.

Competing interests. The contact author has declared that none of the authors has any competing interests.

Disclaimer. Publisher's note: Copernicus Publications remains neutral with regard to jurisdictional claims in published maps and institutional affiliations.

Acknowledgements. We thank Irina Djouraev for the sediment preparation and ICP-MS analysis and the crew and scientists aboard R/V *Meteor* cruises M77/2 in 2008. We deeply thank Bo Thamdrup, chief scientist of the Galathea-3 expedition (Leg 14), and Bente Lomstein, who conducted the core sampling onboard the RV *Vaedderen*.

Financial support. This research has been supported by the Département Soutien et Formation, Institut de Recherche pour le Développement (Bourse ARTS and Contrat de Recherche en Partenariat Laboratoire Mixte International de l'IRD grants), the Consejo Nacional de Ciencia, Tecnología e Innovación Tecnológica (MAGNET Program of CONCYTEC, grant no. 007-2017), the Deutsche Forschungsgemeinschaft (Collaborative Research Project 754 "Climate–Biogeochemistry interactions in the Tropical Ocean" grant), and BELMONT FORUM PACMEDY (grant no. ANR-15-JCLI-0003-03).

Review statement. This paper was edited by Claudio Latorre and reviewed by two anonymous referees.

References

Bahr, A., Hoffmann, J., Schönfeld, J., Schmidt, M., Nürnberg, D., Batenburg, S., and Voigt, S.: Low-latitude expressions of high-latitude forcing during Heinrich Stadial 1 and the Younger Dryas in northern South America, Global Planet. Change, 160, 1–9, https://doi.org/10.1016/j.gloplacha.2017.11.008, 2018.

Baker, P. A., Seltzer, G. O., Fritz, S. C., Dunbar, R. B., Grove, M. J., Tapia, P. M., Cross, S. L., Rowe, H. D., and Broda, J. P.: The History of South American Tropical Precipitation for the Past 25 000 Years, Science, 291, 640–643, https://doi.org/10.1126/science.291.5504.640, 2001a.

Baker, P., Rigsby, C., Seltzer, G., Fritz, S., Lowenstein, T., Bacher, N., and Veliz, C.: Tropical climate changes at millennial and orbital timescales on the Bolivian Altiplano, Nature, 409, 698–701, https://doi.org/10.1038/35055524, 2001b.

Bellomo, K., Angeloni, M., Corti, S., and von Hardenberg, J.: Future climate change shaped by inter-model differences in Atlantic meridional overturning circulation response, Nat. Commun., 12, 1–10, https://doi.org/10.1038/s41467-021-24015-w, 2021.

Beuscher, S., Krüger, S., Ehrmann, W., Schmiedl, G., Milker, Y., Arz, H., and Schulz, H.: End-member modelling as a tool for climate reconstruction – An Eastern Mediterranean case study, PLoS ONE, 12, e0185136, https://doi.org/10.1371/journal.pone.0185136, 2017.

Blard, P., Sylvestre, F., Tripati, A., Claude, C., Causse, C., Coudrain, A., Condom, T., Seidel, J., Vimeux, F., Moreau, C., Dumoulin, J., and Lavé, J.: Lake highstands on the Altiplano (Tropical Andes) contemporaneous with Heinrich 1 and the Younger Dryas: new insights from ^{14}C, U–Th dating and δ^{18}O of carbonates, Quaternary Sci. Rev., 30, 3973–3989, https://doi.org/10.1016/j.quascirev.2011.11.001, 2011.

Bourrel, L., Rau, P., Dewitte, B., Labat, D., Lavado, W., Coutaud, A., Vera, A., Alvarado, A., and Ordoñez, J.: Low-frequency modulation and trend of the relationship between ENSO and precipitation along the northern to centre Peruvian Pacific coast, Hydrol. Process., 29, 1252–1266, https://doi.org/10.1002/hyp.10247, 2015.

Briceño-Zuluaga, F. J., Sifeddine, A., Caquineau, S., Cardich, J., Salvatteci, R., Gutierrez, D., Ortlieb, L., Velazco, F., Boucher, H., and Machado, C.: Terrigenous material supply to the Peruvian central continental shelf (Pisco, 14° S) during the last 1000 years: paleoclimatic implications, Clim. Past, 12, 787–798, https://doi.org/10.5194/cp-12-787-2016, 2016.

Briceño-Zuluaga, F., Castagna, A., Rutllant, J. A., Flores-Aqueveque, V., Caquineau, S., Sifeddine, A., Velazco, F., Gutierrez, D., and Cardich, J.: Paracas dust storms: Sources, trajectories and associated meteorological conditions, Atmos. Environ., 165, 99–110, https://doi.org/10.1016/j.atmosenv.2017.06.019, 2017.

Caesar, L., Rahmstorf, S., Robinson, A., Feulner, G., and Saba, V.: Observed fingerprint of a weakening Atlantic Ocean overturning circulation, Nature, 556, 191–196, https://doi.org/10.1038/s41586-018-0006-5, 2018.

Cardich, J., Sifeddine, A., Salvatteci, R., Romero, D., Briceño-Zuluaga, F., Graco, M., Anculle, T., Almeida, C., and Gutiérrez, D.: Multidecadal Changes in Marine Subsurface Oxygenation Off Central Peru During the Last ca. 170 Years, Front. Mar. Sci., 6, 270, https://doi.org/10.3389/fmars.2019.00270, 2019.

Chamorro, A., Echevin, V., Colas, F., Oerder, V., Tam, J., and Quispe-Ccalluari, C.: Mechanisms of the intensification of the upwelling-favorable winds during El Niño 1997–1998 in the Peruvian upwelling system, Clim. Dynam., 51, 3717–3733, https://doi.org/10.1007/s00382-018-4106-6, 2018.

Cheng, H., Sinha, A., Wang, X., Cruz, F. W., and Edwards, R. L.: The Global Paleomonsoon as seen through speleothem records from Asia and the Americas, Clim. Dynam., 39, 1045–1062, https://doi.org/10.1007/s00382-012-1363-7, 2012.

Cheng, H., Sinha, A., Cruz, F., Wang, X., Edwards, R., d'Horta, F., Ribas, C., Vuille, M., Stott, L., and Auler, A.: Climate change patterns in Amazonia and biodiversity, Nat. Commun., 4, 1–6, https://doi.org/10.1038/ncomms2415, 2013.

Clark, P. U., Shakun, J. D., Baker, P. A., Bartlein, P. J., Brewer, S., Brook, E., Carlson, A. E., Cheng, H., Kaufman, D. S., and Liu, Z.: Global climate evolution during the last deglaciation, P. Natl. Acad. Sci. USA, 109, E1134–E1142, https://doi.org/10.1073/pnas.1116619109, 2012.

Cruz, F. W., Burns, S. J., Karmann, I., Sharp, W. D., Vuille, M., Cardoso, A. O., Ferrari, J. A., Silva Dias, P. L., and Viana, O.: Insolation-driven changes in atmospheric circulation over the past 116 000 years in subtropical Brazil, Nature, 434, 63–66, https://doi.org/10.1038/nature03365, 2005.

Deplazes, G., Lückge, A., Peterson, L. C., Timmermann, A., Hamann, Y., Hughen, K. A., Röhl, U., Laj, C., Cane, M. A., and Sigman, D. M.: Links between tropical rainfall and North Atlantic climate during the last glacial period, Nat. Geosci., 6, 213–217, https://doi.org/10.1038/ngeo1712, 2013.

Dewitte, B., Illig, S., Renault, L., Goubanova, K., Takahashi, K., Gushchina, D., Mosquera, K., and Purca, S.: Modes of covariability between sea surface temperature and wind stress intraseasonal anomalies along the coast of Peru from satellite observations (2000–2008), J. Geophys. Res.-Oceans, 116, C4, https://doi.org/10.1029/2010jc006495, 2011.

Dypvik, H. and Harris, N.: Geochemical facies analysis of fine-grained siliciclastics using Th/U, Zr/Rb and (Zr + Rb)/Sr ratios, Chem. Geol., 181, 131–146, https://doi.org/10.1016/s0009-2541(01)00278-9, 2001.

Echevin, V., Colas, F., Espinoza-Morriberon, D., Vasquez, L., Anculle, T., and Gutierrez, D.: Forcings and Evolution of the 2017 Coastal El Niño Off Northern Peru and Ecuador, Front. Mar. Sci., 5, 367, https://doi.org/10.3389/fmars.2018.00367, 2018.

Fleury, S., Martinez, P., Crosta, X., Charlier, K., Billy, I., Hanquiez, V., Blanz, T., and Schneider, R. R.: Pervasive multidecadal variations in productivity within the Peruvian Upwelling System over the last millennium, Quat. Sci. Rev., 125, 78–90, https://doi.org/10.1016/j.quascirev.2015.08.006, 2015.

Flores-Aqueveque, V., Caquineau, S., Alfaro, S., Valdes, J., and Vargas, G.: Using Image-Based Size Analysis For Determining the Size Distribution and Flux of Eolian Particles Sampled In Coastal Northern Chile (23 S), J. Sediment. Res., 84, 238–244, https://doi.org/10.2110/jsr.2014.23, 2014.

Flores-Aqueveque, V., Alfaro, S., Vargas, G., Rutllant, J. A., and Caquineau, S.: Aeolian particles in marine cores as a tool for quantitative high-resolution reconstruction of upwelling favorable winds along coastal Atacama Desert, Northern Chile, Prog. Oceanogr., 134, 244–255, https://doi.org/10.1016/j.pocean.2015.02.003, 2015.

Garreaud, R., Vuille, M., Compagnucci, R., and Marengo, J.: Present-day South American climate, Palaeogeogr. Palaeocl., 281, 180–195, https://doi.org/10.1016/j.palaeo.2007.10.032, 2009.

González-Pinilla, F., Latorre, C., Rojas, M., Houston, J., Rocuant, M., Maldonado, A., Santoro, C., Quade, J., and Betancourt, J.: High- and low-latitude forcings drive Atacama Desert rainfall variations over the past 16,000 years, Sci. Adv., 7, 38, https://doi.org/10.1126/sciadv.abg1333, 2021.

Gutiérrez, D., Sifeddine, A., Reyss, J. L., Vargas, G., Velazco, F., Salvatteci, R., Ferreira, V., Ortlieb, L., Field, D., Baumgartner, T., Boussafir, M., Boucher, H., Valdés, J., Marinovic, L., Soler, P., and Tapia, P.: Anoxic sediments off Central Peru record interannual to multidecadal changes of climate and upwelling ecosystem during the last two centuries, Adv. Geosci., 6, 119–125, https://doi.org/10.5194/adgeo-6-119-2006, 2006.

Gutiérrez, D., Sifeddine, A., Field, D. B., Ortlieb, L., Vargas, G., Chávez, F. P., Velazco, F., Ferreira, V., Tapia, P., Salvatteci, R., Boucher, H., Morales, M. C., Valdés, J., Reyss, J.-L., Campusano, A., Boussafir, M., Mandeng-Yogo, M., García, M., and Baumgartner, T.: Rapid reorganization in ocean biogeochemistry off Peru towards the end of the Little Ice Age, Biogeosciences, 6, 835–848, https://doi.org/10.5194/bg-6-835-2009, 2009.

Gutiérrez, D., Bouloubassi, I., Sifeddine, A., Purca, S., Goubanova, K., Graco, M., Field, D., Méjanelle, L., Velazco, F., Lorre, A., Salvatteci, R., Quispe, D., Vargas, G., Dewitte, B., and Ortlieb, L.: Coastal cooling and increased productivity in the main upwelling zone off Peru since the mid-twentieth century, Geophys. Res. Lett., 38, 7, https://doi.org/10.1029/2010GL046324, 2011.

Guzman, E., Ramos, C., and Dastgheib, A.: Influence of the El Niño Phenomenon on Shoreline Evolution. Case Study: Callao Bay, Perú, J. Mar. Sci. Eng., 8, 90, https://doi.org/10.3390/jmse8020090, 2020.

Holz, C., Stuut, J. B. W., Henrich, R., and Meggers, H.: Variability in terrigenous sedimentation processes off northwest Africa and its relation to climate changes: Inferences from grain-size distributions of a Holocene marine sediment record, Sediment. Geol., 202, 499–508, https://doi.org/10.1016/j.sedgeo.2007.03.015, 2007.

Humphries, M. S., Benitez-Nelson, C. R., Bizimis, M., and Finch, J. M.: An aeolian sediment reconstruction of regional wind intensity and links to larger scale climate variability since the last deglaciation from the east coast of southern Africa, Global Planet. Change, 156, 59–67, https://doi.org/10.1016/j.gloplacha.2017.08.002, 2017.

Jansen, J., Van der Gaast, S., Koster, B., and Vaars, A.: CORTEX, a shipboard XRF-scanner for element analyses in split sediment cores, Mar. Geol., 151, 143–153, https://doi.org/10.1016/s0025-3227(98)00074-7, 1998.

Jarvis, K. E., Gray, A. L., and Houk, R. S.: Handbook of Inductively Coupled Plasma Mass Spectrometry, 1st edn., Springer, Netherlands, ISBN: 978-94-010-5355-6, 1992.

Jiang, H., Zhong, N., Li, Y., Ma, X., Xu, H., Shi, W., Zhang, S., and Nie, G.: A continuous 13.3-ka record of seismogenic dust events in lacustrine sediments in the eastern Tibetan Plateau, Sci. Rep., 7, 1–10, https://doi.org/10.1038/s41598-017-16027-8, 2017.

Just, J., Heslop, D., von Dobeneck, T., Bickert, T., Dekkers, M. J., Frederichs, T., Meyer, I., and Zabel, M.: Multiproxy characterization and budgeting of terrigenous end-members at the NW African continental margin, Geochem. Geophys. Geosyst., 13, 9, https://doi.org/10.1029/2012GC004148, 2012.

Koutavas, A. and Joanides, S.: El Niño-Southern Oscillation extrema in the Holocene and Last Glacial Maximum, Paleoceanography, 27, 4, https://doi.org/10.1029/2012pa002378, 2012.

Lagos, P., Silva, Y., Nickl, E., and Mosquera, K.: El Niño – related precipitation variability in Perú, Adv. Geosci., 14, 231–237, https://doi.org/10.5194/adgeo-14-231-2008, 2008.

Mamalakis, A., Randerson, J., Yu, J., Pritchard, M., Magnusdottir, G., Smyth, P., Levine, P., Yu, S., and Foufoula-Georgiou, E.: Zonally contrasting shifts of the tropical rain belt in response to climate change, Nat. Clim. Change, 11, 143–151, https://doi.org/10.1038/s41558-020-00963-x, 2021.

Martin, L. C. P., Blard, P. H., Lavé, J., Condom, T., Prémaillon, M., Jomelli, V., Brunstein, D., Lupker, M., Charreau, J., Mariotti, V., Tibari, B., Team, A., and Davy, E.: Lake Tauca highstand (Heinrich Stadial 1a) driven by a southward shift of the Bolivian High, Sci. Adv., 4, 8, https://doi.org/10.1126/sciadv.aar2514, 2018.

McGee, D., Donohoe, A., Marshall, J., and Ferreira, D.: Changes in ITCZ location and cross-equatorial heat transport at the Last Glacial Maximum, Heinrich Stadial 1, and the mid-Holocene, Earth Planet. Sci. Lett., 390, 69–79, https://doi.org/10.1016/j.epsl.2013.12.043, 2014.

McManus, J. F., Francois, R., Gherardl, J. M., Kelgwin, L., and Drown-Leger, S.: Collapse and rapid resumption of Atlantic meridional circulation linked to deglacial climate changes, Nature, 428, 834–837, https://doi.org/10.1038/nature02494, 2004.

Mollier-Vogel, E., Leduc, G., Böschen, T., Martinez, P., and Schneider, R. R.: Rainfall response to orbital and millennial forcing in northern Peru over the last 18 ka, Quat. Sci. Rev., 76, 29–38, https://doi.org/10.1016/j.quascirev.2013.06.021, 2013.

Montade, V., Kageyama, M., Combourieu-Nebout, N., Ledru, M. P., Michel, E., Siani, G., and Kissel, C.: Teleconnection between the intertropical convergence zone and southern westerly winds throughout the last deglaciation, Geology, 43, 735–738, https://doi.org/10.1130/G36745.1, 2015.

Morera, S., Condom, T., Crave, A., Steer, P., and Guyot, J.: The impact of extreme El Niño events on modern sediment transport along the western Peruvian Andes (1968–2012), Sci. Rep., 7, 1–14, https://doi.org/10.1038/s41598-017-12220-x, 2017.

Mulitza, S., Chiessi, C. M., Schefuß, E., Lippold, J., Wichmann, D., Antz, B., Mackensen, A., Paul, A., Prange, M., Rehfeld, K., Werner, M., Bickert, T., Frank, N.,

Kuhnert, H., Lynch-Stieglitz, J., Portilho-Ramos, R. C., Sawakuchi, A. O., Schulz, M., Schwenk, T., Tiedemann, R., Vahlenkamp, M., and Zhang, Y.: Synchronous and proportional deglacial changes in Atlantic meridional overturning and northeast Brazilian precipitation, Paleoceanography, 32, 622–633, https://doi.org/10.1002/2017PA003084, 2017.

Ng, H. C., Robinson, L. F., McManus, J. F., Mohamed, K. J., Jacobel, A. W., Ivanovic, R. F., Gregoire, L. J., and Chen, T.: Coherent deglacial changes in western Atlantic Ocean circulation, Nat. Commun., 9, 1–10, https://doi.org/10.1038/s41467-018-05312-3, 2018.

Novello, V. F., Cruz, F. W., Vuille, M., Stríkis, N. M., Edwards, R. L., Cheng, H., Emerick, S., de Paula, M. S., Li, X., Barreto, E. de S., Karmann, I., and Santos, R. V.: A high-resolution history of the South American Monsoon from Last Glacial Maximum to the Holocene, Sci. Rep., 7, 44267, https://doi.org/10.1038/srep44267, 2017.

Ortlieb, L., Vargas, G., and Saliège, J. F.: Marine radiocarbon reservoir effect along the northern Chile-southern Peru coast (14–24° S) throughout the Holocene, Quat. Res., 75, 91–103, https://doi.org/10.1016/j.yqres.2010.07.018, 2011.

Paterson, G. A. and Heslop, D.: New methods for unmixing sediment grain size data, Geochem. Geophys. Geosyst., 16, 4494–4506, https://doi.org/10.1002/2015GC006070, 2015.

Peterson, L., Haug, G., Hughen, K., and Röhl, U.: Rapid Changes in the Hydrologic Cycle of the Tropical Atlantic During the Last Glacial, Science, 290, 1947–1951, https://doi.org/10.1126/science.290.5498.1947, 2000.

Pettijohn, F.: Persistence of Heavy Minerals and Geologic Age, J. Geol., 49, 610–625, https://doi.org/10.1086/624992, 1941.

Pichevin, L., Cremer, M., Giraudeau, J., and Bertrand, P.: A 190 ky record of lithogenic grain-size on the Namibian slope: Forging a tight link between past wind-strength and coastal upwelling dynamics, Mar. Geol., 218, 81–96, https://doi.org/10.1016/j.margeo.2005.04.003, 2005.

Rahmstorf, S., Box, J., Feulner, G., Mann, M., Robinson, A., Rutherford, S., and Schaffernicht, E.: Exceptional twentieth-century slowdown in Atlantic Ocean overturning circulation, Nat. Clim. Change, 5, 475–480, https://doi.org/10.1038/nclimate2554, 2015.

Rahn, D. and Garreaud, R.: A synoptic climatology of the near-surface wind along the west coast of South America, Int. J. Climatol., 34, 780–792, https://doi.org/10.1002/joc.3724, 2013.

Rau, P., Bourrel, L., Labat, D., Melo, P., Dewitte, B., Frappart, F., Lavado, W., and Felipe, O.: Regionalization of rainfall over the Peruvian Pacific slope and coast, Int. J. Climatol., 37, 143–158, https://doi.org/10.1002/joc.4693, 2016.

Rein, B., Lückge, A., and Sirocko, F.: A major Holocene ENSO anomaly during the Medieval period, Geophys. Res. Lett., 31, 7, https://doi.org/10.1029/2004gl020161, 2004.

Rein, B., Lückge, A., Reinhardt, L., Sirocko, F., Wolf, A., and Dullo, W. C.: El Niño variability off Peru during the last 20 000 years, Paleoceanography, 20, 4, https://doi.org/10.1029/2004PA001099, 2005.

Reinhardt, L., Kudrass, H. R., Lückge, A., Wiedicke, M., Wunderlich, J., and Wendt, G.: High-resolution sediment echosounding off Peru: Late Quaternary depositional sequences and sedimentary structures of a current-dominated shelf, Mar. Geophys. Res., 23, 335–351, 2002.

Salvatteci, R., Gutiérrez, D., Field, D., Sifeddine, A., Ortlieb, L., Bouloubassi, I., Boussafir, M., Boucher, H., and Cetin, F.: The response of the Peruvian Upwelling Ecosystem to centennial-scale global change during the last two millennia, Clim. Past, 10, 715–731, https://doi.org/10.5194/cp-10-715-2014, 2014a.

Salvatteci, R., Field, D., Sifeddine, A., Ortlieb, L., Ferreira, V., Baumgartner, T., Caquineau, S., Velazco, F., Reyss, J., Sanchez-Cabeza, J., and Gutierrez, D.: Cross-stratigraphies from a seismically active mud lens off Peru indicate horizontal extensions of laminae, missing sequences, and a need for multiple cores for high resolution records, Mar. Geol., 357, 72–89, https://doi.org/10.1016/j.margeo.2014.07.008, 2014b.

Salvatteci, R., Gutierrez, D., Sifeddine, A., Ortlieb, L., Druffel, E., Boussafir, M., and Schneider, R.: Centennial to millennial-scale changes in oxygenation and productivity in the Eastern Tropical South Pacific during the last 25 000 years, Quat. Sci. Rev., 131, 102–117, https://doi.org/10.1016/j.quascirev.2015.10.044, 2016.

Salvatteci, R., Schneider, R. R., Blanz, T., and Mollier-Vogel, E.: Deglacial to Holocene Ocean Temperatures in the Humboldt Current System as Indicated by Alkenone Paleothermometry, Geophys. Res. Lett., 46, 281–292, https://doi.org/10.1029/2018GL080634, 2019.

Saukel, C., Lamy, F., Stuut, J. B. W., Tiedemann, R., and Vogt, C.: Distribution and provenance of wind-blown SE Pacific surface sediments, Mar. Geol., 280, 130–142, https://doi.org/10.1016/j.margeo.2010.12.006, 2011.

Scheidegger, K. F. and Krissek, L. A.: Dispersal and deposition of eolian and fluvial sediments off Peru and northern Chile., Geol. Soc. Am. Bull., 93, 150–162, https://doi.org/10.1130/0016-7606(1982)93<150:DADOEA>2.0.CO;2, 1982.

Shakun, J. D., Clark, P. U., He, F., Marcott, S. A., Mix, A. C., Liu, Z., Otto-Bliesner, B., Schmittner, A., and Bard, E.: Global warming preceded by increasing carbon dioxide concentrations during the last deglaciation, Nature, 484, 49–54, https://doi.org/10.1038/nature10915, 2012.

Sifeddine, A., Gutierrez, D., Ortlieb, L., Boucher, H., Velazco, F., Field, D., Vargas, G., Boussafir, M., Salvatteci, R., Ferreira, V., García, M., Valdés, J., Caquineau, S., Mandeng Yogo, M., Cetin, F., Solis, J., Soler, P., and Baumgartner, T.: Laminated sediments from the central Peruvian continental slope: A 500 year record of upwelling system productivity, terrestrial runoff and redox conditions, Prog. Oceanogr., 79, 190–197, https://doi.org/10.1016/j.pocean.2008.10.024, 2008.

Stríkis, N., Cruz, F., Barreto, E., Naughton, F., Vuille, M., Cheng, H., Voelker, A., Zhang, H., Karmann, I., Edwards, R., Auler, A., Santos, R., and Sales, H.: South American monsoon response to iceberg discharge in the North Atlantic, P. Natl. Acad. Sci. USA, 115, 3788–3793, https://doi.org/10.1073/pnas.1717784115, 2018.

Stríkis, N. M., Chiessi, C. M., Cruz, F. W., Vuille, M., Cheng, H., De Souza Barreto, E. A., Mollenhauer, G., Kasten, S., Karmann, I., Edwards, R. L., Bernal, J. P., and Sales, H. D. R.: Timing and structure of Mega-SACZ events during Heinrich Stadial 1, Geophys. Res. Lett., 42, 5477–5484, https://doi.org/10.1002/2015GL064048, 2015.

Strub, P. T., Mesias, J. M., Montecino, V., Rutllant, J., and Salinas, S.: Coastal ocean circulation off western South America, in: The Sea, Vol. 11, edited by: Robinson, A. and Brink, K., John Wiley & Sons, New York, USA, 273–313, ISBN: 0-471-1154-2, 1998.

Stuut, J. B. W. and Lamy, F.: Climate variability at the southern boundaries of the Namib (southwestern Africa) and Atacama (northern Chile) coastal deserts during the last 120 000 yr, Quat. Res., 62, 301–309, https://doi.org/10.1016/j.yqres.2004.08.001, 2004.

Stuut, J. B. W., Prins, M. A., Schneider, R. R., Weltje, G. J., Fred Jansen, J. H., and Postma, G.: A 300-kyr record of aridity and wind strength in southwestern Africa: Inferences from grain-size distributions of sediments on Walvis Ridge, SE Atlantic, Mar. Geol., 180, 221–233, https://doi.org/10.1016/S0025-3227(01)00215-8, 2002.

Stuut, J. B. W., Kasten, S., Lamy, F., and Hebbeln, D.: Sources and modes of terrigenous sediment input to the Chilean continental slope, Quat. Int., 161, 67–76, https://doi.org/10.1016/j.quaint.2006.10.041, 2007.

Stuut, J. B. W., Temmesfeld, F. and De Deckker, P.: A 550 ka record of aeolian activity near north west cape, australia: Inferences from grain-size distributions and bulk chemistry of SE indian ocean deep-sea sediments, Quat. Sci. Rev., 83, 83–94, https://doi.org/10.1016/j.quascirev.2013.11.003, 2014.

Sublette Mosblech, N., Chepstow-Lusty, A., Valencia, B., and Bush, M.: Anthropogenic control of late-Holocene landscapes in the Cuzco region, Peru, The Holocene, 22, 1361–1372, https://doi.org/10.1177/0959683612449760, 2012.

Suess, E., Kulm, L. D., and Killingley, J. S.: Coastal upwelling and a history of organic-rich mudstone deposition off Peru, Geol. Soc. Spec. Publ., 26, 181–197, https://doi.org/10.1144/GSL.SP.1987.026.01.11, 1987.

Vuille, M., Burns, S. J., Taylor, B. L., Cruz, F. W., Bird, B. W., Abbott, M. B., Kanner, L. C., Cheng, H., and Novello, V. F.: A review of the South American monsoon history as recorded in stable isotopic proxies over the past two millennia, Clim. Past, 8, 1309–1321, https://doi.org/10.5194/cp-8-1309-2012, 2012.

Weltje, G. J. and Prins, M. A.: Muddled or mixed? Inferring palaeoclimate from size distributions of deep-sea clastics, Sediment. Geol., 162, 39–62, https://doi.org/10.1016/s0037-0738(03)00235-5, 2003.

Weltje, G. J. and Prins, M. A.: Genetically meaningful decomposition of grain-size distributions, Sediment. Geol., 202, 409–424, https://doi.org/10.1016/j.sedgeo.2007.03.007, 2007.

Wu, L., Wilson, D., Wang, R., Yin, X., Chen, Z., Xiao, W., and Huang, M.: Evaluating Zr/Rb Ratio From XRF Scanning as an Indicator of Grain-Size Variations of Glaciomarine Sediments in the Southern Ocean, Geochem. Geophy. Geosy., 21, 11, https://doi.org/10.1029/2020gc009350, 2020.

Yarincik, K., Murray, R., and Peterson, L.: Climatically sensitive eolian and hemipelagic deposition in the Cariaco Basin, Venezuela, over the past 578 000 years: Results from Al/Ti and K/Al, Paleoceanography, 15, 210–228, https://doi.org/10.1029/1999pa900048, 2000.

Zhang, Y., Chiessi, C. M., Mulitza, S., Zabel, M., Trindade, R. I. F., Helena, M., Hollanda, B. M., Dantas, E. L., Govin, A., Tiedemann, R., and Wefer, G.: Origin of increased terrigenous supply to the NE South American continental margin during Heinrich Stadial 1 and the Younger Dryas, Earth Planet. Sci. Lett., 432, 493–500, https://doi.org/10.1016/j.epsl.2015.09.054, 2015.

Zhou, W., Leung, L., Lu, J., Yang, D., and Song, F.: Contrasting Recent and Future ITCZ Changes From Distinct Tropical Warming Patterns, Geophys. Res. Lett., 47, 22, https://doi.org/10.1029/2020gl089846, 2020.